

Photoinduced Electron-Transfer in 2-*tert*-Butyl-3-(Anthracen-9-yl)-2,3-Diazabicyclo[2.2.2]octane*

Guadalupe Valverde-Aguilar¹, Jorge Garcia-Macedo¹, Xianghuai Wang², Jeffrey I. Zink² Stephen F. Nelsen³

¹ Instituto de Física, UNAM. Circuito exterior 04510. Cd. Universitaria Coyoacán. México D.F. E-mail: valverde@chem.ucla.edu Phone: (5255) 56225103, FAX: (5255) 56161535.

² Department of Chemistry and Biochemistry, University of California, Los Angeles California 90095.

³ Department of Chemistry, University of Wisconsin, 1101 University Avenue, Madison, Wisconsin 53706-1396.

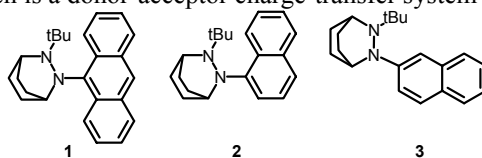
ABSTRACT

Intramolecular photoinduced electron-transfer from a hydrazine unit to an aromatic group is studied by resonance Raman spectroscopy and electronic absorption spectroscopy. Substituted hydrazine functional groups have played an important role in studies of electron transfer reactions, photo-induced intramolecular electron transfer, and of mixed valence. A prototypical compound, 2-*tert*-Butyl-3-(Anthracen-9-yl)-2,3-Diazabicyclo[2.2.2]octane, that has the hydrazine to anthracene charge transfer band in a region of the visible spectrum suitable for detailed resonance Raman spectroscopy is studied in detail. Excitation profiles are obtained, calculated quantitatively by using time-dependent theoretical methods, and interpreted with the assistance of molecular orbital calculations. Excited state distortions are calculated. The largest distortions occur on the hydrazine unit; the normal mode showing the largest distortion (659 cm⁻¹, calculated at 665 cm⁻¹) involves an out of plane C-N-N-C bend consistent with removing an electron from the NN π antibonding orbital. Anthracene ring-centered CC stretches also are enhanced, consistent with populating an antibonding π orbital centered on the ring. Excellent fits to all of the excitation profiles and to the absorption band are obtained using one set of excited state potential surfaces.

Keywords: Raman spectroscopy, absorption, electron-transfer, mixed valence.

1. INTRODUCTION

Photoinduced electron-transfer is a subject that has received intense study.¹⁻³ Absorption of a photon produces an excited state that may have an amount of charge transfer varying from very little to almost complete, although electron transfer may also follow photoexcitations that produce little charge transfer in the initial step. Several of the spectroscopic techniques that are used to study electron transfer upon photoexcitation have been reviewed recently.⁴ In this paper we use resonance Raman (*rR*) spectroscopy, electronic absorption spectroscopy, and the time-dependent theory of spectroscopy⁵⁻⁹ to analyze the photoinduced electron-transfer in 2-*tert*-butyl-3-(anthracen-9-yl)-2,3-diazabicyclo[2.2.2]-octane, **1**, which is a donor-acceptor charge-transfer system where

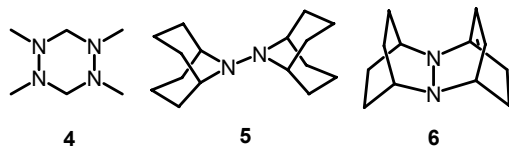


the donor **Hy** is the hydrazine group and the acceptor **AN** is the anthracene group. The excited state has substantial **Hy**⁺-**AN**⁻ charge-transfer character, as has been recently established for **1** and its naphthalene analogues **2** and **3** using electrooptical absorption measurements.¹⁰

Hydrazines have been important in electron transfer studies because they have convincingly established the importance of internal reorganization energy (λ_v) in determining electron transfer rates. Tetraalkylhydrazines have some of the largest λ_v values known because they undergo unusually large geometry changes upon electron loss. Neutral acyclic tetraalkylhydrazines have nitrogens that are pyramidalized past tetrahedral (the average of the heavy atom bond angles, α_{av} being less than 109.5°) and an electronic preference for perpendicular nitrogen lone pairs.¹¹ Hydrazine

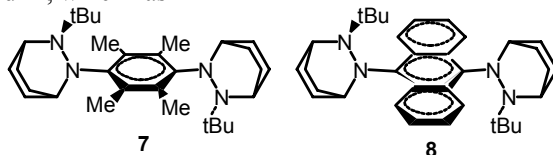
radical cations electronically prefer nitrogens that are nearly planar and have their p-rich lone pair orbitals coplanar for best overlap in the three-electron pi bond.¹²

Bishydrazine **4** has slow electron transfer on the ESR time scale,¹³ which is only



consistent with a major effect of λ_v on the rate constant, because it had been long known that linking lower λ_v charge-bearing units, such as nitrobenzene groups by a single methylene group in the anion of 4,4'-dinitrodiphenylmethane results in rapid intramolecular electron transfer.¹⁴ Electron transfer disproportionation upon approach of two hydrazine radical cations generates dication, neutral pairs with a $\Delta G^\circ_{\text{disp}}$ of about 20 kcal/mol, and the basic neutral oxidation level compound deprotonates the acidic 2+ oxidation level one so rapidly that decomposition occurs at the rate of disproportionation for most examples. The N,N-bicyclic 9-azabicyclo-[3.3.1]nonyl group protects a single nitrogen by forcing both C_{α} -H bonds to lie near the nodal plane of the p-rich orbital at the flattened radical cation, allowing isolation of bis(N,N-bicyclic) hydrazine radical cations such as **5**⁺ and determination of their x-ray structures.¹⁵ Bis(N,N'-bicyclic)-substituted radical cations such as **6**⁺ also proved isolable, and their decreased λ_v values caused by flattening at nitrogen forcing the lone pairs in the neutral form to be coplanar decreased λ_v enough to allow measuring intermolecular self-electron transfer rate constants by NMR line broadening.¹⁶

Obtaining long-lived intervalence bis(hydrazine) radical cations¹⁷ so that their properties could be studied conveniently proved most conveniently done by placing two **Hy** charge-bearing units on aromatic bridges in compounds like the durene diyl bridged **7**⁺, which has



an intramolecular rate constant measured accurately by ESR and an optical spectrum that allowed showing that Hush's evaluation of the electronic coupling H_{ab} accurately predicts the rate constant using classical Marcus-Hush theory.¹⁸ The intervalence bis-**Hy**-substituted analogue of **1**, **8**⁺, has an intramolecular electron transfer rate constant that is about 150 times that of **7**⁺, although comparable rate constants would be expected because their λ and H_{ab} values should be comparable.¹⁹ The optical spectrum of **8**⁺ reveals why – its bridge-oxidized radical cation lies so low in energy that its bridge oxidation transition (**Hy**⁺-**Anth**-**Hy** → **Hy**-**Anth**⁺-**Hy**) lies at lower energy than its intervalence transition (**Hy**⁺-**Anth**-**Hy** → **Hy**-**Anth**-**Hy**⁺), making the two-state model inaccurate.

The analysis of resonance Raman intensities is a powerful tool for determining distortions that molecules undergo upon excitation to excited states and for experimentally obtaining excited-state potential surfaces.²⁰ We have recently employed *rR* to study a delocalized tetraalkyl-p-phenylene diamine radical cation,²¹ an aromatic-bridged dihydrazine diradical dication,²² and an N,N'-diphenyl-hydrazine radical cation.²³ Resonance Raman excitation profiles are especially useful when electronic absorption and emission spectra are unstructured. Although the electronic spectra of large molecules in condensed media contain information about all of the normal modes of the molecule whose potential surface minima are displaced from the minimum of the ground electronic state, the spectra of molecules with many displaced normal modes are frequently so congested that only an unresolved envelope or ill-resolved shoulders are observed.²¹ In contrast, *rR* profiles can be used to obtain information about individual modes because the excited-state information is 'filtered' through the specific normal mode being examined.²⁴ *rR* excitation profiles are a collection of the *rR* intensities of each mode at various excitation wavelengths. To construct the experimental excitation profiles, spectra are taken at various excitation wavelengths in resonance with the absorption band of interest. An internal standard, a molecule that does not absorb at the excitation wavelength being used, is used to obtain the intensity of each vibrational mode relative to that of the standard.

In this paper, *rR* excitation profiles in resonance with the lowest energy absorption band of **1** are measured. The normal modes of vibration that are the most highly distorted are identified and are assigned by using B3LYP calculations. The *rR* intensities and excitation profiles are calculated by using time-dependent theory and the excited state distortions Δ are obtained by fitting the electronic absorption spectrum and the Raman spectra using potential energy surfaces such as those shown in Figure 1 (a) and (b). Both the electronic absorption spectrum and the *rR* profiles

are calculated by using exactly the same potential surfaces.²⁴ The most highly distorted modes involve bond angle and length changes on the hydrazine nitrogen bonded to the anthracene.

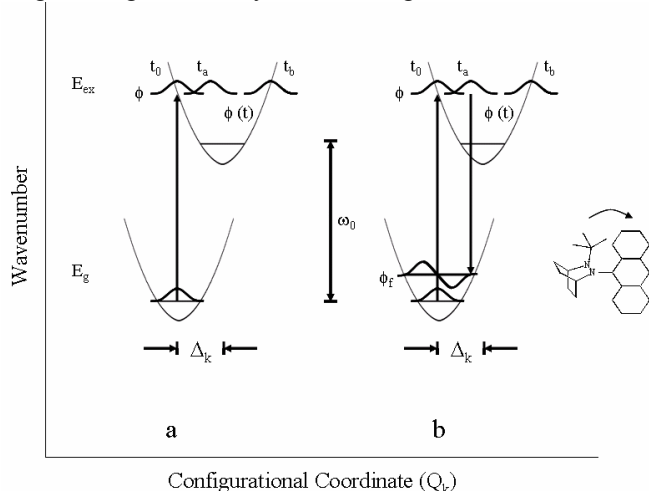


Figure 1. Ground and excited state potential energy surfaces for hydrazine-to-naphthalene electron transfer in **1**. Potential surface (a) illustrates the time-dependent theory of electronic absorption, and (b) that of resonance Raman spectroscopy.

2. EXPERIMENTAL SECTION

Preparation of **1** and characterization by X-ray crystallography have been previously published.²⁵ Absorption spectra of **1** in toluene solution and a KBr pellet were obtained at room temperature using a Cary 5000 UV-Vis-NIR spectrophotometer. Raman spectra were obtained using a 1401 Spex double monochromator equipped with a Burle C31034 photomultiplier tube and a Stanford Research Systems SR400 photon counter, and by using an ISA triple monochromator with a CCD. Excitation was provided by an argon ion laser (for wavelengths of 514.5, 488, 457.9 nm) and a krypton ion laser (for wavelengths of 406.7, 530.9, 568.2, and 676.4 nm). Spectra were collected from spinning pellets made from a finely ground mixture of **1** and NaNO₃ as reference at a ratio of 1:0.03. The intensities were obtained by numerically integrating the peaks. The Raman intensities were normalized to that of the NaNO₃ standard.

3. THEORETICAL AND NUMERICAL METHODS

The time-dependent theory of electronic and resonance Raman spectroscopy is used to analyze and interpret the spectra. It offers a powerful method of calculating spectra in terms of potential surfaces of any form. The theoretical foundation has been well reviewed; the equations used to calculate the spectra are briefly presented in this section.

The fundamental equation for the calculation of an absorption spectrum in the time-dependent theory^{14,15} is eq. (1),

$$I(\omega) = C\omega \int_{-\infty}^{+\infty} \exp(i\omega t) \left\langle \Phi | \Phi(t) \right\rangle \exp\left(-\Gamma t + \frac{iE_0}{\hbar} t\right) dt \quad (1)$$

where $I(\omega)$ as the absorption intensity at frequency ω , E_0 is the energy of the electronic origin transition, and Γ is a phenomenological damping factor. The damping factor arises because of relaxation into other modes (such as low-frequency solvent modes with small distortions) and the bath. The effect of increasing Γ on the spectrum in the frequency domain is to decrease the resolution, that is, to “fill in” the spectrum. The most important ingredient to eq. 1 is $\langle \Phi | \Phi(t) \rangle$, the autocorrelation function of the wave packet Φ prepared on an excited-state potential surface after the spectroscopic transition, with the wave packet $\Phi(t)$ developing on this surface with time. In the absence of coupling terms between the normal coordinates, the total autocorrelation in a system with K coordinates is given by equation (2), where ϕ^k is a wave packet associated

$$\left\langle \Phi | \Phi(t) = \prod_k \langle \phi^k | \phi^k(t) \right\rangle \quad (2)$$

with coordinate k ($k=1, \dots, K$). The initial wave packet is the vibrational wave function times the transition dipole from the ground state electronic surface.

A resonance Raman excitation profile, taken at resonance with an excited electronic state of interest, can be used to determine the magnitude of the distortion of the mode that is measured in the profile. Because each normal mode

can be examined individually in the Raman experiment, the distortion along each of the normal modes can be calculated. Whereas the electronic spectrum contains information about all of the modes simultaneously, the resonance Raman contains the desired information about of a specific mode. The Raman scattering cross section is given by eq. (3)

$$\alpha_{fi} = \frac{i}{\hbar} \int_0^{\infty} \left(\sum_{r=1}^n \mu_r^2 \langle \phi_f | \phi(t) \rangle_r \exp(-iE_{00}^{(r)}t - \Gamma^{(r)}t) \right) \exp\{i(\omega_i + \omega_f)t\} dt \quad (3)$$

where $|\phi_f\rangle = \mu|\chi_f\rangle$ is the final vibrational state χ_f multiplied by the transition electric dipole moment μ , $|\phi(t)\rangle = \exp(-iH_{ex}t/\hbar)|\phi\rangle$ is a moving wave packet propagated by the Hamiltonian, $|\phi\rangle = \mu|\chi\rangle$ is the initial vibrational state multiplied by the electronic transition moment, Γ is the damping factor, $\hbar\omega_i$ is the zero point energy of the ground electronic surface, and $\hbar\omega_f$ is the energy of the incident radiation. The Raman intensity $I_{i \rightarrow f}$ into a particular mode f is given by eq. (4), where ω_s is the frequency of the scattered radiation.

$$I_{i \rightarrow f} \sim \omega_I \omega_s^3 [\alpha_{fi}]^* [\alpha_{fi}] \quad (4)$$

4. RESULTS

The absorption spectrum of **1** in toluene solution at room temperature is shown in Figure 2 (dotted line). The spectrum contains bands at $21830 \pm 100 \text{ cm}^{-1}$ (458 nm), 26390 ± 100

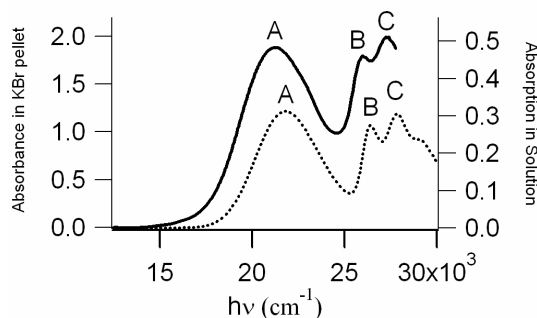


Figure 2. Absorption spectra of **1** at room temperature in toluene at $2 \times 10^{-4} \text{ M}$ (dotted line), in a KBr pellet (solid line).

cm^{-1} (379 nm) and $27860 \pm 100 \text{ cm}^{-1}$ (359 nm), labeled A, B and C, respectively. In a KBr pellet at room temperature, the bands appear at $21230 \pm 100 \text{ cm}^{-1}$ (471 nm), $25970 \pm 100 \text{ cm}^{-1}$ (385 nm) and $27250 \pm 100 \text{ cm}^{-1}$ (367 nm). The first band maximum of the compound in a KBr pellet is shifted by 600 cm^{-1} to lower energy than that in the solution spectrum. The second absorption region (B,C) is attributed to vibronic components of the lowest energy anthracene π, π^* band, which does not have electron transfer character.

Figure 3 shows the Raman spectra of **1** obtained at excitation wavelengths of 514.5 nm and 457.9 nm. Table 1 lists the Raman modes with intensities at least 10% of that of the most intense sample peak (1403 cm^{-1}) observed in the 514.5 nm Raman spectrum. The majority of the modes decrease in intensity when the excitation frequency is changed from 514.5 to 457.9 nm excitation.

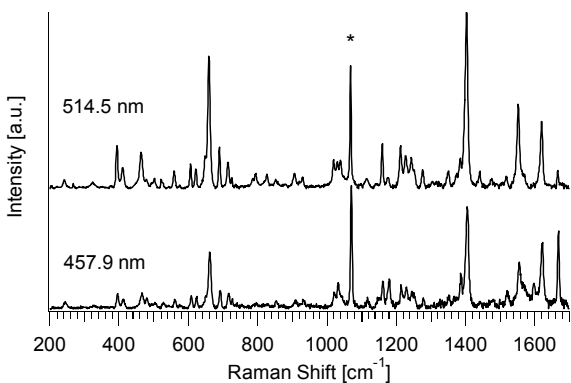


Figure 3. Raman spectra of **1** with 514.5 nm (above) and 457.9 nm (below) excitation. The peak marked * at 1067 cm^{-1} is the NaNO_3 reference peak.

Table 1. Raman Frequencies, Distortions and Assignments

ω_{exp} (cm^{-1})	I_{514}/I_{ref}	Δ	δ (\AA)	ω_{cal}^a (cm^{-1})	Description
241	0.10	1.14	0.25	235	AL C-NN bend + in-plane AN def
325	0.17	1.10	0.20	324	Out of plane AN def
392	0.45	1.50	0.21	397	In plane AN def
410	0.23	1.01	0.16	418	Out of plane AN def
463	0.55	1.40	0.19	465	CNNC bend
558	0.21	0.72	0.09	530	CNNC bend
605	0.22	0.68	0.09	571	CNNC bend + out of plane AL def
620	0.20	0.63	0.061	657	In plane AN def.
659	1.57	1.66	0.18	665	CNNC out of plane bend
689	0.39	0.80	0.073	703	In plane AN def.
713	0.28	0.65	0.066	722	AL C-NNC def + NN str.
1019	0.14	0.33	0.036	1024	AL C-N str.
1030	0.06	0.21	0.026	1062	AL C-NNC def + NN str.
1159	0.43	0.50	0.052	1143	AN C-N str.
1212	0.41	0.46	0.069	1202	AN C-N str.
1227	0.23	0.34	0.044	1264	
1243	0.35	0.42	0.044	1282	AN CC str.
1276	0.25	0.35	0.040	1286	AN CC str.
1351	0.24	0.32	0.030	1364	AN C-N str. + AN CC str.
1403	2.917	1.065	0.0586	1441	AN C-N str. + AN CC str.
1552	0.954	0.551	0.0339	1570	AN CC str. + NNC bend
1620	1.011	0.543	0.0293	1603	AN CC str.

a) AL = aliphatic bicyclo[2.2.2]octane group; AN = anthracene; def = deformation; str. = stretch.

Plots of the integrated Raman intensities as a function of the excitation energy (the resonance Raman excitation profiles) are given in the Figure 4. In order to generate the excitation profiles, it is necessary to employ an intensity standard that does not absorb in the range of excitation wavelengths used. NaNO_3 was chosen as the internal standard. The intensities of the bands of **1** (relative to that of the NaNO_3 standard peak at 1067 cm^{-1}) obtained by exciting at 514.5 nm (19436 cm^{-1} , the wavelength that produces the maximum Raman intensities) are listed in Table 1. The excitation profiles of the bands with the biggest distortions are plotted in Figure 4 with error bars. The spectra that were used to construct the profiles were obtained using $676.4, 568.2, 530.9, 514.5, 488.0, 457.9,$ and 406.7 nm excitations.

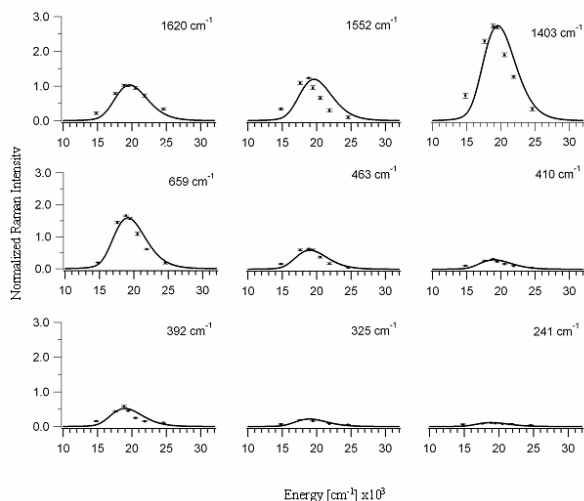


Figure 4. Resonance Raman excitation profiles of the nine most enhanced normal modes. The experimental points are shown with experimental uncertainty bars, and the calculated fits shown as solid lines. All experimental and calculated plots are shown on the same scale.

5. DISCUSSION

The lowest energy absorption band of **1** and those of the naphthalene analogues **2** and **3** were recently characterized using electrooptical absorption measurements.¹⁰ All three compounds were shown to have **Hy-to-Ar** charge transfer character for their lowest energy absorption bands. The change in dipole moment upon absorption ($\Delta\mu_{12}$) for **1** in dioxane was measured to be 4.0 ± 0.4 Debye, corresponding to a charge separation in the excited state of 0.84 ± 0.09 Å on the adiabatic surfaces and 1.27 ± 0.06 Å on the diabatic surfaces, which is slightly less than the 1.43 ± 0.08 obtained for **2** on its diabatic surfaces. The severe N-C_{Ar} twisting caused by steric interactions between the bulky hydrazine and the aryl ring appears to be involved in limiting the amount of charge separation, because the less twisted **3** gave a charge separation on its diabatic surfaces in its excited state of 2.06 ± 0.04 Å. The hydrazine-to-anthracene charge transfer assignment is supported by molecular orbital calculations, which indicate a mixed but predominantly hydrazine π character for the *homo* and significantly more anthracene π^* character to the *lumo*, so excitation transfers charge from the hydrazine unit to the anthracene ring (see Figure 5).

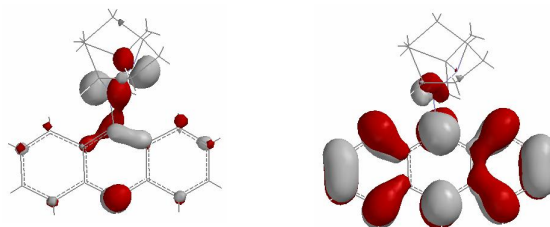
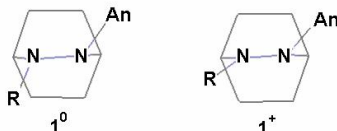


Figure 5. *Homo* (left) and *lumo* (right) for **1**, drawn at Isoval of 0.06 using Spartan'02.²⁶

The vibrations were assigned using UB3LYP/6-31G* calculations²⁷ and were viewed using the MOLDEN software package.²⁸ Scheme 1 shows the geometry change calculated to occur when **1** is oxidized to **1⁺**, which we use as a model for that which occurs upon



Scheme 1. Geometry change involved for electron removal from **1**.

photoexcitation. The geometry change involved for electron removal from **1** has been measured by x-ray crystallography of **1** and **1⁺Ph₄B⁻**.^{10,29} A 0.094 Å (6.5%) shortening of the NN bond (from 1.542(4) to 1.358(2) Å), a 0.021 Å (1.4%) shortening of the NC_{Ar} bond (from 1.495(4) to 1.437(4) Å), a 3.8° (36% of the 10.5° change between tetrahedral and planar) increase in the average CNC bond angles at the N-aryl nitrogen (α_{av} 114.7 to 118.5°) and 6.8° (65%) increase at the N-tert-butyl nitrogen (α_{av} 112.3 to 119.1°), an increase in the twist angle about the N-C_{Ar} bond from 43.2(4)° to 66.7(2)°, and an increase in the lone pair, lone pair twist angle as the nitrogens flatten from 126.8(3)° to 157.0(1) occur upon electron removal.

The lowest energy electronic transition transfers charge from the *homo*, which is heavily centered on the hydrazine unit, to the *lumo* which is principally anthracene ring-centered. Oxidizing a hydrazine removes an NN π^* antibonding electron, which shortens the NN bond length, flattens the nitrogens, and changes the electronic preference for twist at the NN bond from near 90° to 0°. ³⁰⁻³² This transition also weakens the N-C_{Ar} bond because the *homo* is bonding and the *lumo* is antibonding there (see Fig. 5). Motion along coordinates that produce these structural changes will lead to enhanced resonance Raman intensity. The mode with the biggest distortion is the out of plane C-N-N-C bend at 659 (calc. 665) cm⁻¹. The *rR* intensity of this mode is much smaller than that of the symmetric C-N stretch that is observed at 1403 cm⁻¹ (calc. 1441 cm⁻¹), but its distortion is larger because Δ_k scales as the square root of the intensity and the inverse square of the frequency. Distortions are also quite large for low-frequency bending modes observed at 241 and 463 cm⁻¹. The modes 1243 cm⁻¹, 1276 cm⁻¹ and 1620 cm⁻¹ that involve anthracene CC stretching undergo modest distortions (Δ_k of 0.35 to 0.54).

The intensities of the rR bands and their excitation profiles were calculated by using eqs. (4) and (5), and these results are compared with the experimental profiles in Figure 4. The variable parameters that are used in the calculation are the damping Γ and the distortions. For each normal coordinate, its frequency, ω , and distortion, Δ , define the potential surface. The resonance Raman excitation profiles for the ten-dimensional surface are calculated using $\phi(t)$ according to eqs. (2-4). The intensity of each excitation profile in Figure 4 is roughly proportional to $\omega^2 \Delta^2$. Only one set of parameters is used to calculate all of the excitation profiles, to calculate the resonance Raman spectrum at a given excitation wavelength, and to calculate the absorption spectrum as discussed in last section. The nine spectra were fit simultaneously using the distortions shown in Table 1 and $\Gamma = 500 \text{ cm}^{-1}$. A full-width at half-maximum (FWHM) of $5,503 \text{ cm}^{-1}$ was obtained.

The Δ values given in Table 1 are dimensionless distortions. Conversion to Angstrom units provides more physical meaning to these distortions. The conversion is given in equation (5), where δ is the bond length change in angstroms, Δ is the dimensionless

$$\delta = 10^8 \Delta \sqrt{\frac{6.023 \times 10^{23}}{m} \frac{\hbar}{2\pi c \omega}} \quad (5)$$

distortion along the normal coordinate, ω is the frequency of the vibrational mode in cm^{-1} , m is the mass of the vibration in molecular mass units, \hbar is Plank's constant in $\text{g cm}^2 \text{ s}^{-1}$ divided by 2π , and c is the speed of light in cm s^{-1} . The normal masses were obtained from the MO calculation. The δ values calculated using eq. (6) are also listed in Table 1.

The absorption spectrum of **1** was calculated by using eq. (1) with the parameters determined from the rR profiles. The calculated absorption spectrum is shown superimposed on the experimental spectrum in Figure 6. The calculated and experimental spectra are in excellent agreement.

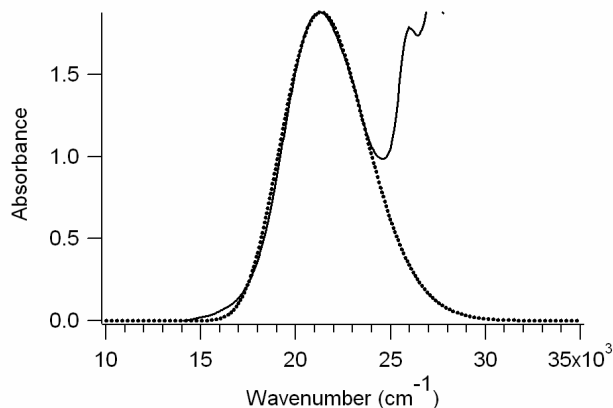


Figure 6. Calculated fit of the absorption spectrum of **1**; the solid line is the experimental spectrum at room temperature in a KBr pellet; the dotted line is the calculated spectrum. The damping factor is 500 cm^{-1} .

6. SUMMARY

The lowest excited state of the hydrazine-substituted anthracene compound arises from a hydrazine to anthracene charge transfer. Molecular orbital calculations show that the *homo* has a predominantly hydrazine π character and that the *lumo* is almost entirely anthracene π^* in character. Resonance Raman excitation profiles taken in resonance with the charge transfer absorption band were used to obtain detailed information about the bond length and angle changes that occur as a result of the charge transfer. The largest distortions occur on the hydrazine unit because oxidizing it removes an NN π^* electron that shortens the NN bond length, flattens the nitrogens, and changes the electronic preference for twist at the NN bond from nearly 90° to 0° . The normal mode showing the largest distortion (659 cm^{-1} , calculated at 665 cm^{-1}) involves an out of plane C-N-N-C bend consistent with the expected change. Anthracene ring-centered CC stretches, consistent with populating an antibonding pi orbital centered on the ring also are enhanced. The magnitudes of the normal coordinate changes are calculated using the time-dependent theory of resonance Raman spectroscopy. Excellent fits to all of the excitation profiles and to the absorption band are obtained using one set of parameters. Details of the individual normal mode changes and thus the geometrical changes that the widely used hydrazine functional group undergoes upon photo-induced electron transfer are provided by the interpretation of the resonance Raman profiles.

Acknowledgments. This work was made possible by grants from the National Science Foundation, CHE-0240197 (SFN), CHE-0507929 (JIZ), CONACYT 43226-F, NSF-CONACYT and DGAPA UNAM IN111902 and PAPIIT

116506-3. SFN acknowledges gifts from the Intel Corporation and grant CHE0091916 from the NSF for support of the departmental computers used in this work. GVA is grateful for a UCMEXUS- CONACYT post-doctoral fellowship.

REFERENCES

- ¹ J. F. Endicott, *Electron Transfer in Chemistry*, Eds. Balzani, V. ; Piotrowiak, P. Wiley-VCH: Weinheim, Germany, Vol. 1, Part 1, Chapter 7, 238-270, 2001.
- ² S. M. Hubig; J. K. Kochi, *Electron Transfer in Chemistry*, Eds. Balzani, V. ; P. Astruk, D, Wiley-VCH: Weinheim, Germany, Vol. 2, Part 2, Chapter 2, 518-676, 2001.
- ³ M. N. Paddon-Row, *Electron Transfer in Chemistry*, Ed. Balzani, V. Wiley-VCH: Weinheim, Germany, Vol. 3, Part 2, Chapter 1, 179-271, 2001.
- ⁴ K. Henbest; M. A. J. Rodgers, *Electron Transfer in Chemistry*, Eds. Balzani, V. ; Rodgers, M. A. J. Wiley-VCH: Weinheim, Germany, Vol. 1, Part 2, Chapter 4, 558-588, 2001.
- ⁵ C. Reber; J.I. Zink, *Comments Inorg. Chem.*, 13, 177 (1992).
- ⁶ K.-S. K. Shin; J.I. Zink, *Inorg. Chem.* 28, 4358 (1989).
- ⁷ D. Wexler; Zink, J.I.; C. Reber, In *Electronic and Vibronic Spectra of Transition Metal Complexes I*, H. Yersin, editor (Berlin, Heidelberg: Springer-Verlag,), 174, 1994.
- ⁸ A. Acosta,; J. I. Zink, *J. Organom. Chem.* 554, 87 (1998).
- ⁹ A. Myers Kelley, *J. Phys. Chem. A* 103, 6891 (1999).
- ¹⁰ S. A. E. Konradsson, M. N. Weaver, I. Guzei, M. Göbel, R. Wortmann, J. V. Lockard, J. I. Zink. *J. Phys. Chem. A* 109, 10854-10861 (2005).
- ¹¹ S.F. Nelsen, in *Acyclic Organonitrogen Stereodynamics*, Lambert, J.B.; Takeuchi, Y., Eds., VCH: New York, Chapter 3, p. 89-121, 1992,
- ¹² S.F. Nelsen, in *Acyclic Organonitrogen Stereodynamics*, Lambert, J.B.; Takeuchi, Y., Eds., VCH: New York, NY, Chapter 7, p. 245-262, 1992.
- ¹³ S. F. Nelsen, P. J. Hintz, J. M. Buschek, G. R. Weisman *J. Am. Chem. Soc.* 97, 4933-4936, (1975).
- ¹⁴ J. E. Harriman, A. H. Maki *J. Chem. Phys.* 39, 778-786, (1963).
- ¹⁵ (a) S. F. Nelsen, W. C. Hollinsed, C. R. Kessel, J.C. Calabrese *J. Am. Chem. Soc.* 100, 7876-7882 (1978). (b) S. F. Nelsen, G. T. Cunkle, D. H. Evans, K. J. Haller, M. Kaftory, B. Kirste, T. Clark *J. Am. Chem. Soc.* 107, 3829-3839 (1985).
- ¹⁶ (a) S. F. Nelsen, S. C. Blackstock, *J. Am. Chem. Soc.* 107, 7189-7190 (1985). (b) S. F. Nelsen, T. B. Frigo, Y. Kim, S. B. Blackstock, *J. Am. Chem. Soc.* 111, 5387-5397 (1989). (c) S. F. Nelsen, Y. Wang *J. Org. Chem.* 59, 1655-1662 (1994).
- ¹⁷ (a) S. F. Nelsen, M. R. Willi, J. M. Mellor, N. M. Smith, *J. Org. Chem.* 51, 2081-2089 (1986). (b) S. F. Nelsen, H. Chang, J. J. Wolff, J. Adamus *J. Am. Chem. Soc.* 115, 12276-12289 (1993).
- ¹⁸ (a) S. F. Nelsen, R. F. Ismagilov, D. R. Powell *J. Am. Chem. Soc.* 119, 10213-10222 (1997). (b) For a review, see S. F. Nelsen *Adv. Phys. Org. Chem.*, to be published.
- ¹⁹ S. F. Nelsen, R. F. Ismagilov, D. R. Powell *J. Am. Chem. Soc.* 120, 1924-1925 (1998).
- ²⁰ R. J. H. Clark, R. E. Hester, Ed. *Advances in Infrared and Raman Spectroscopy*; Wiley: Chichester, 1975-1989; Vols. 1-17 and references therein. R. J. H. Clark, T. Dines *J. Angew. Chem., Int. Ed. Engl.* 1986, 25, 13, and references therein.
- ²¹ S. E. Bailey, J. I. Zink, S. F. Nelsen *J. Am. Chem. Soc.* 125, 5939-5947 (2003).
- ²² J. V. Lockard, J. I. Zink, A. E. Konradsson, M. N. Weaver, S. F. Nelsen *J. Am. Chem. Soc.* 125, 13471-13480 (2003).
- ²³ J. V. Lockard, J. I. Zink, D. A. II Trieber, A. E. Konradsson, M. N. Weaver, S. F. Nelsen *J. Phys. Chem. A* 109, 1205-1215 (2005).
- ²⁴ K. S. Shin, R. J. H. Clark, J. I. Zink *J. Am. Chem. Soc.* 112, 3754 (1990).
- ²⁵ S.F. Nelsen, R. F. Ismagilov, D. R. Powell *JACS* 120, 1924 (1998).
- ²⁶ Spartan '02, Wavefunction, Inc., Irvine, California.
- ²⁷ M. J. Frish, et al. Gaussian 03, Revision C.02; Gaussian, Inc. Wallingford CT 2004.
- ²⁸ G. Schaftenaar, J.H. Noordik *J. Comput.-Aided Mol. Design* 14, 123 (2000).
- ²⁹ S. F. Nelsen, A. E. Konradsson, R. F. Ismagilov, I. A. Guzei, *Crystal Growth & Design* 6, 2344-2347 (2005).
- ³⁰ N S. F. elsen, *Acct. Chem. Res.* 14, 131-138 (1981).
- ³¹ S. F. Nelsen, in *Molecular Structures and Energetics*; J. F. Liebman, A. Greenberg, Eds.; VCH Publishers, Inc.: Deerfield Beach, FL, Vol. 3, Ch. 1, pp.1-56, 1986.
- ³² S.F. Nelsen, in *Acyclic Organonitrogen Stereodynamics*, J.B. Lambert, Y. Takeuchi, Eds., VCH: New York, NY, Chapter 7, p. 245-262, 1992.